Transactions of the **13th International Conference on Structural Mechanics in Reactor Technology** (SMiRT 13), Escola de Engenharia - Universidade Federal do Rio Grande do Sul, Porto Alegre, Brazil, August 13-18, 1995

Probabilistic finite element analysis for structural fragility evaluation

Ghiocel, D.M., Wilson, P.R., Stevenson, J.D.
Stevenson & Associates Inc., Ohio, U.S.A.

ABSTRACT: Recently new advanced numerical techniques have been developed for probabilistic nonlinear finite element analyses. One of these, used herein, is the Advanced Mean Value (AMV) procedure developed by Wu et al., 1990, also included in the NASA NESSUS code. The paper presents the structural fragility evaluation of a reactor vessel Concrete Cavity (CC) and a Containment Structure (CS) of a nuclear Reactor Building (RB) under accidental overpressure load using the AMV procedure. The most significant parameters were considered as random variables with different types of distributions. Static and dynamic structural analyses were performed. To investigate the dynamic structural behavior in the transient regime first the possible critical instant times were determined. Fragility curves (conditional probability of failure vs. peak pressure) and associated probability density functions were computed for the structural failure modes of each structure. Fitted lognormal formats including both the randomness and uncertainty random variabilities of design parameters were developed. The overall system fragilities were finally computed by combining the structural failure mode fragilities.

1 INTRODUCTION

Because of the catastrophic consequence of a nuclear station failure and of the large potential hazards associated with nuclear plants the evaluation of the probabilities of failure represents a key issue related to nuclear safety. One of the major considerations in evaluating radioactive releases in the probabilistic risk assessment of nuclear power plants is the integrity of the Concrete Cavity (CC) and the Containment Structure (CS). Herein the structural fragility of these two structures to accidental internal overpressure loads is investigated.

The reactor vessel CC is a cylindrical reinforced concrete thick shell which encloses in its interior space the reactor pressure vessel. Its concrete wall and basemat are 3 ft thick. The cavity is surrounded by the RB basemat which is 10 ft thick. Between the cavity wall and RB basemat there is a steel liner which interrupts the concrete continuity. The CS is a large cylindrical wall covered by a flat spherical dome. The containment structure is a partially prestressed reinforced concrete shell with a 110 ft interior diameter. The wall is 3 ft - 10 1/2 in thick and the dome is 3 ft thick.

Detailed 3D axisymmetric computational models including the RB basemat and the surrounding soil foundation were used to model the CC and the CS. These finite element structural models were used to identify the global (burst) failure modes of the investigated structures and determine the associated fragility curves. Local failures, especially near equipment hatches were analyzed using local models having as boundary conditions the displacements determined from the global models and are not presented herein.

The reliability based finite element computations were performed using the ANSYS code. Pre- and post- processor codes for reliability evaluations were developed in-house and interfaced with the ANSYS code. The contact (gap and sliding) type of nonlinearities were included. For comparative purposes a nonlinear material finite element analysis of the CS was performed with the SOLVIA code (similar to ADINA code) using a concrete axisymmetric finite element.

2 RELIABILITY ANALYSIS PROCEDURE

The Advanced Mean Value (AMV) procedure (Wu et al., 1990) was used for the reliability evaluation. This procedure is computationally efficient and gives relatively accurate results for practical engineering purposes, especially for limit state (response) functions having small nonlinearity. For the investigated problem the AMV procedure was chosen to reduce the computational effort involved by the dynamic transient analysis in which the reliability evaluations are repeated for several critical time steps.

For a given failure or limit state function $\mathbf{Z(X)}$ the AMV response function model Z_{AMV} is given by the expression (Wu et al., 1990):

$$Z_{AMV}(\mathbf{X}) = Z_{MV}(\mathbf{X}) + H(Z_{MV}) \tag{1}$$

where $Z_{MV}(\mathbf{X})$ is the mean-point linearized approximation of the limit state function and $H(Z_{MV})$ is defined as the difference between the exact limit state function and its mean-point linearized function calculated at the Most-Probable Point (MPP). The following six computational steps were performed: (1) Derive of the mean-point linearized limit state function $Z_{MV}(\mathbf{X})$, (2) Determine the MPP, $\mathbf{X^*}$, (3) Compute the value of the linearized limit state function at the MPP, $Z_{MV}(\mathbf{X^*})$, (4) Compute the exact limit state function at MPP, $Z(\mathbf{X^*})$, by an additional finite element analysis (5) Evaluate the difference $H(Z_{MV})=Z(\mathbf{X^*})-Z_{MV}(\mathbf{X^*})$ and (6) Compute the limit state function using equation (1). The approximation involved by the AMV procedure is that the slope of the limit state function at the MPP is considered to be equal to the slope at the mean point. To evaluate the partial derivatives of the limit state function parametric variations of the mean point values were considered. Larger variations are not recommended if the approximate location of the MPP is not previously known.

For non-normal variables equivalent normal distributions were first derived. The mean and standard deviation of the equivalent normal variables are determined such that at the value X_i^*, the cumulative probability and probability density of the actual non-normal and the equivalent normal variable are equal. To evaluate fragility curves (conditional failure probability versus mean pressure intensity) for the CC and CS, repeated reliability analyses were performed. For the CS, final fragility curves based on a lognormal format were computed using fitted lognormal distributions. Lognormal distributions were fitted for fragility curves and the corresponding medians, $\tilde{x}$, and logarithmic standard deviations β_r were estimated using the expressions:

$$\tilde{x} = \exp\left(\sum_i f_i \ln x_i\right)$$

$$\beta_r = \left[\sum_i f_i (\ln x_i - \sum_i f_i \ln x_i)\right]^{1/2} \tag{2}$$

The random variabilities coming from randomness and modeling uncertainty were considered separately. Using lognormal format, fragility curves with 5, 50, and 95 percent confidence levels were computed. System fragility curves for the major significant failure modes were determined by combining them. For the system fragility evaluation perfect correlations or zero correlations between failure modes were assumed based on engineering judgments.

3 REACTOR CAVITY UNDER LOCALIZED OVERPRESSURE

A detailed 3D axisymmetric finite element ANSYS model was used to compute the stresses in the reactor vessel CC under a high pressure impulsive load as shown in Figure 1. The computational model includes the CC and also the RB basemat and the surrounding soil foundation. The cavity may slide on the RB basemat, no shear stresses being transmitted through the interface between them. Contact finite elements were used.

The overpressure load inside the nuclear reactor vessel cavity was described by a triangular impulse with a total duration of 0.005 seconds. The peak pressure, the rise time and the decay time of the triangular impulse were considered as random variables. The spatial pressure distribution was defined by an uniform distribution over 6 ft on the wall, from 2.4 ft to 8.4 ft height. The distributions and statistics of the random variables are given in Table 1.

The displacement (ft) and stress (psf) time histories (evolution in seconds) were computed for selected nodes and elements. The dynamic deformed shape of the cavity at time 0.0036 sec., which corresponds to the highest maximum displacement and shear stress is shown in Figure 2. The maximum sectional effects were determined by integration of the stresses over sectional areas at different time steps. The maximum sectional forces per structural element in the cavity and RB basemat (critical sections for shear failure) are shown in Table 2. In parenthesis are given the DLF (Dynamic Load Factors defined as ratios of the dynamic resonse to static response). Their values vary from 0.48 to 2.40. For the shear forces in the CC the DLF are 0.48 for the wall and 1.25 for the base.

Table 3 shows the mean forces and mean strengths in critical sections for different structural failure modes of the cavity. Mean safety factors and capacities in terms of pressure load intensity were also computed. The mean safety factors vary between 1.05 to 8.38. The critical failure modes were the concrete shear failures of the base wall and of the lateral wall of the CC, which have safety factors of 1.05 and 1.83, respectively. However, a realistic safety margin has to include the presence of the adjacent RB basemat. If the shear strength of the adjacent RB basemat is considered then the mean safety factors for shear failures become 3.18-3.45 (written in parenthesis in Table 4). The global safety factors including failures of both the cavity wall and RB basemat were computed assuming that the shear forces were transferred entirely from the cavity to the RB basemat after the failure of the concrete cavity.

The mean shear strengths and safety factors for the RB basemat computed for the assumptions of no cavity failure and cavity failure are shown in Table 4. If the CC does not fail, the safety factors were considerably greater, being 4.93 and 5.73. These differences show the strong dependence between the shear failure of the cavity wall and the failure of the RB basemat.

For the evaluation of concrete shear strengths for sections subjected to membrane tensions, a modified ACI CC-3000 Design formula was used:

$$v_c = C_0\sqrt{f_c'}\,(1 + 0.002N_u / A_g) \qquad (3)$$

where f_c' is the concrete compressive strength, C_0 is the shear strength coefficient, N_u is the axial force, and A_g is the concrete cross-sectional area.

The focus of the reliability analysis was the critical shear failure modes (including the effect of axial force) of the concrete cavity. The shear failures considered were: CCH and CCV denoting the shear failures of the concrete cavity in horizontal and vertical sections (the presence of RB basemat is ignored), and RBHF and RBVF denoting the shear failures of the adjacent RB basemat in horizontal and vertical directions given the failure of the cavity. The cavity and the RB basemat were considered as parallel subsystems. The structural system fails when both components fail. The safety indices and fragility curves of the critical shear failure modes are shown in Figure 3. The global shear failure modes of both the CC and the RB basemat are denoted with CRBH and CRBV, which correspond to the last two curves on the right hand side of the fragility curve graphs. It should be noted that the mean pressure capacity is still larger than 3000 psi for both the CRBH and CRBV failure modes.

4 CONTAINMENT STRUCTURE UNDER INTERNAL OVERPRESSURE

The 3D axisymmetric model used to idealize the containment structure is shown in Figure 4a. Both static and dynamic linear analyses were performed using the ANSYS code. The static internal overpressure was considered uniformly distributed on the inner surface of the containment including also a part of the basemat region near the wall. The dynamic internal pressure was modeled by a time evolution described by a triangular impulse decaying to a constant pressure value of 15% of the peak pressure. The total duration of the triangular impulse was 0.01 seconds. The deformed shape of the containment at the maximum displacement time is shown in Figure 4b. The aging effect of the 20 years on the concrete strength was taken into account by a factor equal to 1.8. Pressure load, prestressing forces and sectional capacities were modeled as random variables as defined in Table 6. Herein only the static results are presented.

The containment shell failure is dominated by three failure modes: (i) tension failure due to high membrane forces in the hoop direction in the cylinder above the mid-height, (ii) tension failure in hoop/meridional direction due to high membrane forces in the dome at the center and (ii) shear failure due to shear forces at the base of the cylinder, near the joint with the base mat. The results of the fragility analyses expressed in the lognormal format are given in Table 7. The controlling failure mode, with the lowest median capacity, was the membrane tension failure in the cylinder wall in the hoop direction near the mid-height. The system fragility was determined from the individual failure mode fragilities assuming statistically independent failure modes. The system fragility curve and its associated probability density function are plotted in Figure 6. The overall median capacity of the containment was found to be close to 215 psi (3.58 times the design pressure P_D = 60 psi). If the interdependencies between failure modes are considered the failure analysis becomes more complex as shown by the nonlinear analysis presented next.

An additional nonlinear finite element analysis using finite element concrete elements was performed to investigate in more depth the failure mechanism of the containment under an internal overpressure load (Figure 5). Only the median design parameters were considered. Herein, the nonlinear finite element analysis was performed using SOLVIA/PC Version 90.2 code. The results of this nonlinear analysis show a significant interaction between the different failure modes. The first yielding occurs in the hoop rebars slightly above mid-height of cylinder wall, followed by yielding in meridional direction of the liner near the wall joints. The concrete is completely cracked for pressures higher than 130 psi. Above 160 psi pressure, a significant increase of radioactive release is expected through large concrete cracks in the wall. The overall ultimate median pressure capacity is estimated to be 205 psi (3.42 x P_D), which is only slightly lower value than 215 psi determined by linear analyses.

Using the results of the fragility analyses shown in Table 7 the overall High Confidence Low Probability of Failure (HCLPF) pressure capacity of the containment was estimated to be around 130 psi (2.17 design pressure). The above values for median capacities refer to the structural capacity of the concrete containment and not to its functional capacity to prevent leakage. The leakage through the wall is expected to be significant above 160 psi.

REFERENCES

Ghiocel, D.M., Wilson P., Stevenson, J.D., 1995. Structural Fragility of A Nuclear Power Plant Reactor Vessel and Containment Using Finite Element Computational Models, The 36 th Conference on Structures, Structural Dynamics and Materials, Section on Probabilistic Applications, New Orleans

Wu,Y.I., Millwater, H., Cruse,T.A. 1990. Advanced Probabilistic Structural Analysis Method for Implicit Performance Functions ", AIAA Journal, Vol.28,nr.9

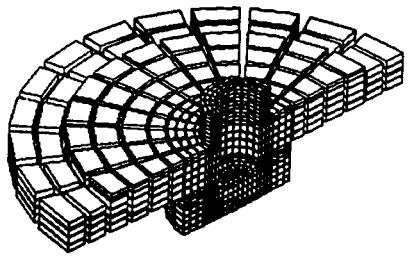

Figure 1. Concrete Cavity (CC) model

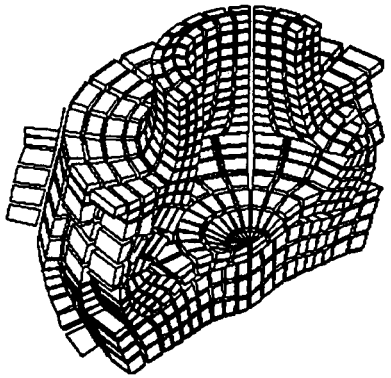

Figure 2. Deformed shape of the cavity

Table 1. Statistical parameters of random variables

Variable	Distribution	Mean	C.O.V.
Peak Pressure (P)	Extreme Type I	variable psi	0.20
Total Duration (Td)	Normal	0.005 sec.	0.20
Raise Time (Tr)	Normal	0.0025 sec.	0.20
Soil Stiffness (K)	Lognormal	16.95 E+10 lb/ft	0.30
Concrete Strength (f'_c)	Lognormal	5000 psi	0.10
Concrete Shear Strength Coefficient (Coef)	Normal	3.0	0.20

Table 2. Sectional Forces for 1000 psi Pressure Load (Dynamic)

Structure	Element	Axial force (lb)	Hoop force (lb)	Shear force (lb)	Bending Moment (lb-in)
Concrete	Base	131486 (1.44)	134557 (1.45)	22668 (1.25)	55655 (2.40)
Cavity	Wall	32340 (negative)	315643 (1.23)	70458 (0.48)	171915 (0.57)
RB	Under cavity	90988 (1.52)	88896 (1.54)	36132 (1.42)	137176 (0.94)
Basemat	Adjacent to cavity wall	-54834 (0.99)	120808 (1.14)	34757 (0.82)	208107 (1.70)

Table 3. Mean Safety Factors and Mean Capacities for the Concrete Cavity

Element	Failure mode	Mean Force	Mean Strength	Safety Factors	Mean Capacity (pressure)
Base	Axial Tension	131486lb	660000lb	5.02	5020 psi
	Hoop Tension	134557lb	660000lb	4.90	4900 psi
	Shear Failure	22668lb	23900 lb	1.05 (3.18)	1050 psi (3180 psi)
Wall	Concrete Compression	1042 psi	5000 psi	4.80	4800 psi
	Axial Tension	102528lb	858000lb	8.37	8370 psi
	Hoop Tension	315643lb	2647500lb	8.38	8380 psi
	Shear Failure	70758lb	129390lb	1.83 (3.45)	1830 psi (3450 psi)

Table 4. Safety Factors and Mean Capacities for Shear Failures of the RB basemat

Section		Mean force (lb)	Mean strength (lb)	Safety Factors	Mean Capacity (pressure)
Vertical, under cavity	- no cavity failure	36132	178164	4.93	4930 psi
	- cavity failure	58800		3.03	3030 psi
Horizontal, adjacent to cavity	- no cavity failure	34757	199315	5.73	5730 psi
	- cavity failure	105215		1.89	1890 psi

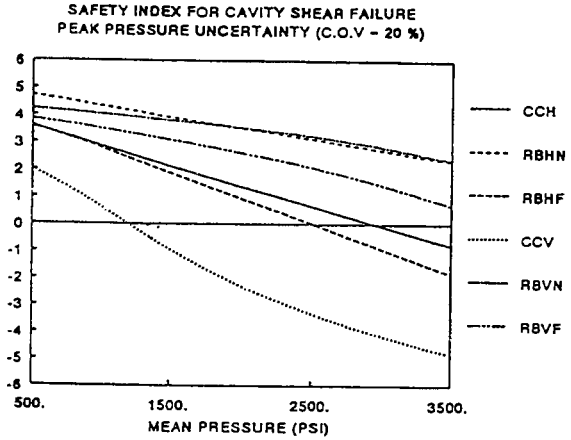

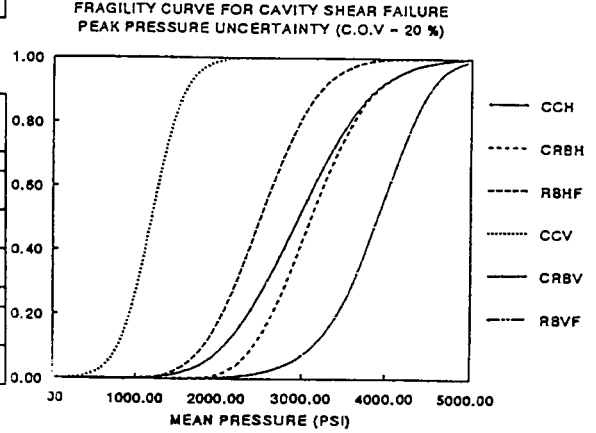

Figure 3. Safety indices and fragility curves

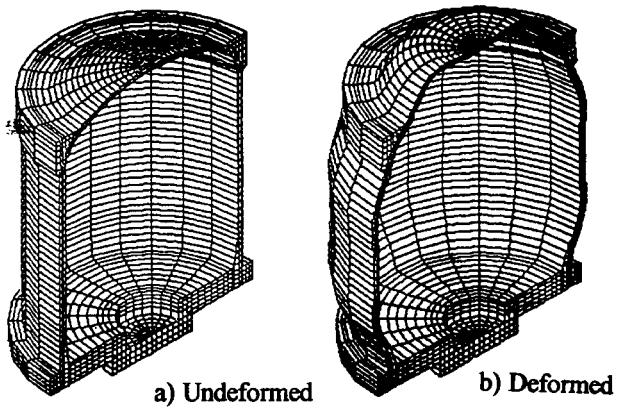

Figure 4. Containment Structure (CS)

Table 6. Random variable considered for reliability analyses

Load	Mean	C.o.v.	Distribution
Pressure	Variable in intensity	0.25	Extreme Type I
Prestressing forces	Nominal values x 0.90, including the loss of prestress in time	0.10	Normal
Sectional strength	Mean values for concrete and steel strengths are introduced	0.05 to 0.10	Lognormal

Table 7. Summary of the containment overpressure failure modes

Failure mode	Median Capacity	β_r	β_u	$\beta_i = (\beta_r^2 + \beta_u^2)^{1/2}$	Comments
Hoop tension in cylinder	235 psi	0.12	0.15	0.19	Large hole in the cylinder
Hoop/meridional tension in dome	282 psi	0.11	0.15	0.19	Large hole in the dome
Shear failure in cylinder near base	268 psi	0.11	0.15	0.19	Large crack thru the wall
Meridional tension near ring beam	392 psi	0.08	0.15	0.17	Large hole in the dome
Basemat shear failure near wall	284 psi	0.14	0.16	0.20	Large crack thru basemat
Basemat bending failure near wall	284 psi	0.14	0.14	0.20	Large crack near cylinder
Equipment hatch	310 psi	0.10	0.13	0.16	Large crack thru cylinder

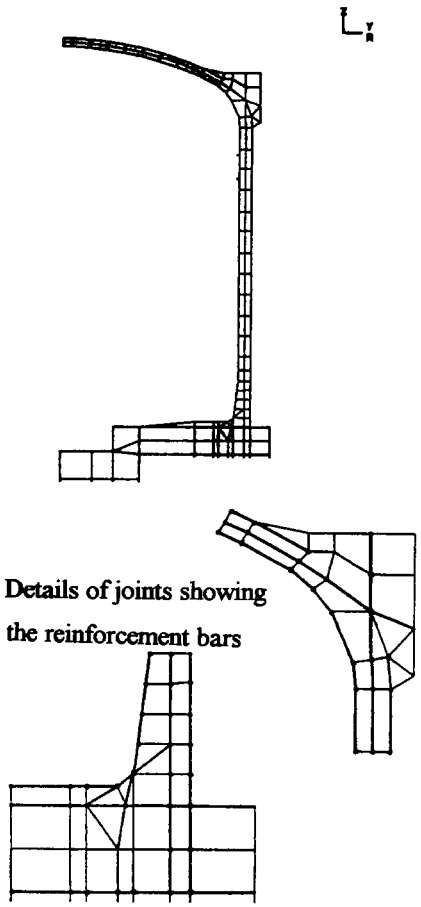

Figure 5. SOLVIA nonlinear model

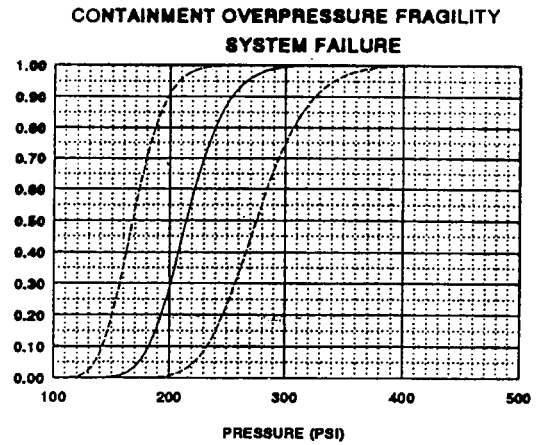

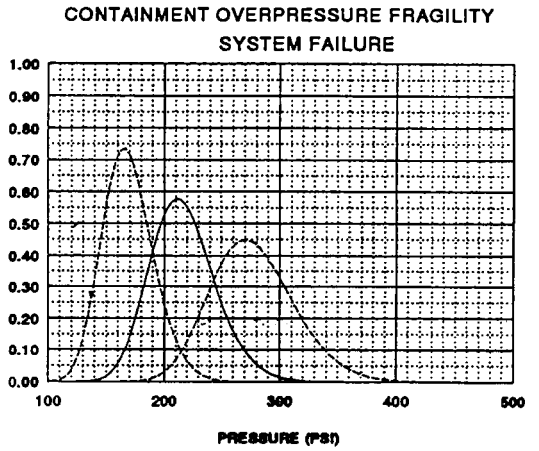

Figure 6. Fragility curves and probability densities